

Protecting benzylic C–H bonds by deuteration doubles the operational lifetime of deep blue Ir-phenylimidazole dopants in phosphorescent OLEDs

Hyejin Bae

Samsung Advanced Institute of Technology

Jong Soo Kim

Samsung Advanced Institute of Technology

Alexander Yakubovich

Samsung R&D Institute Russia (SRR)

Jinhoon Jeong

Korea Advanced Institute of Science and Technology

Sangho Park

Samsung Electronics Co., LTD

Jun Chwae

Samsung Advanced Institute of Technology

Satoko Ishibe

Samsung Advanced Institute of Technology (SAIT)

Won-Joon Son

Samsung Advanced Institute of Technology <https://orcid.org/0000-0003-4087-4661>

Yongsik Jung

Samsung Advanced Institute of Technology <https://orcid.org/0000-0003-4496-2351>

Sunghan Kim

Samsung Advanced Institute of Technology

Hyeonho Choi

Samsung Electronics Co., Ltd. <https://orcid.org/0000-0002-6884-8193>

Mu-Hyun Baik (✉ mbaik2805@kaist.ac.kr)

Korea Advanced Institute of Science and Technology <https://orcid.org/0000-0002-8832-8187>

Article

Keywords: organic light-emitting diodes, benzylic C-H bonds, deep blue Ir-phenylimidazole dopants

Posted Date: November 12th, 2020

DOI: <https://doi.org/10.21203/rs.3.rs-98832/v1>

License:  This work is licensed under a Creative Commons Attribution 4.0 International License.

[Read Full License](#)

Version of Record: A version of this preprint was published at Advanced Optical Materials on May 18th, 2021. See the published version at <https://doi.org/10.1002/adom.202100630>.

Abstract

Much effort has been dedicated to increase the operational lifetime of blue phosphorescent materials in organic light-emitting diodes (OLEDs), but the reported device lifetimes are still too short for the industrial applications. An attractive method for increasing the lifetime of a given emitter without making any chemical change is exploiting the kinetic isotope effect, where key C–H bonds are deuterated. A computer model identified that the most vulnerable molecular site in an Ir-phenylimidazole dopant is the benzylic C–H bond and predicted that deuteration may lower the deactivation pathway involving C–H/D cleavage notably. Experiments showed that the device lifetime (T_{70}) of a prototype phosphorescent OLED device could be doubled to 355 hours with a maximum external quantum efficiency of 25.1% at 1000 cd/m². This is one of the best operational performances of blue phosphorescent OLEDs observed to date in a single stacked cell.

Introduction

Phosphorescent transition metal complexes have attracted much attention as emitting materials in organic light-emitting diodes (OLEDs) due to their short excited state lifetime, and because their internal quantum efficiency can in principle reach 100%.^{1–5} Cyclometalated Ir(III) complexes are particularly interesting, as their color can be tuned over the entire visible range from blue to red.^{6–16} But finding blue phosphorescent materials that are robust enough for industrial applications proved challenging, which may be rationalized by the large band gap^{17–19} compared to red or green emitters, leading to high-energy excited states that are consequently more reactive and are therefore expected to degrade more easily. Such degradation may give rise to short device lifetime and low efficiency. It is therefore necessary to develop blue phosphorescent materials that are chemically much more stable to engineer long device lifetime and high efficiency.

Despite being conceptually easy, it proved difficult to find rational ways of inhibiting the degradation to increase operational lifetime and efficiency.^{20–22} A number of factors such as structural degradation,^{23–25} triplet-polaron,^{26–27} and triplet-triplet annihilation^{28–30} have been considered as potential causes of these inefficiencies, but much remains unclear and a unified strategy for systematically increasing the performance of blue emitters has not emerged. One of the main difficulties in developing systematic strategies lies in the fact that little is known about what causes the loss in activity at the molecular level and a quantitative structure-reactivity relationship could not be established thus far. As a result, optimization efforts cannot build upon a precise mechanistic understanding and must rely on conjecture and empirical observations. For instance, bis(4',6'-difluorophenylpyridinato)iridium(picolate) (FIrpic) is one of the most extensively studied blue dopants in phosphorescent OLEDs.^{31–33} The dissociation of the ancillary picolate ligand and the cleavage of C–F bonds^{34–38} were proposed to be responsible for its deactivation. Consequently, fluorine-free homoleptic blue Ir(III) complexes^{39–42} were prepared, and the ancillary ligand was changed to carbene^{43–45} or pyrimidine^{46–47} functionalities. Ligands were decorated with cyano groups⁴⁰ and pyrimidine moieties were introduced. Fluorine-free, homoleptic phenylimidazole-

based Ir(III) dopants showed promising performance,^{24,41} but the improvement in OLED device lifetimes were only moderate.

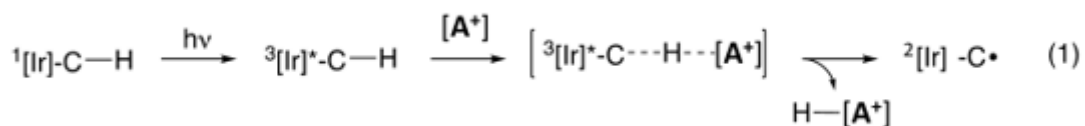
Using the kinetic isotope effect (KIE)⁴⁸ to stabilize emitters is an unusual, but interesting strategy. Unlike conventional methods where the composition of the emitter must be changed to impact its chemical property, replacing an element within a molecule by its heavier isotope does not alter the chemical composition, but renders bond-cleavage reactions slower, which may potentially improve the performance of blue phosphorescent materials. Specifically, if the cleavage of a C–H bond is involved in the rate-determining step of the deactivation reaction, its rate can be lowered by replacing the protium by deuterium. Because the zero point vibrational energy (ZPE) of a C–H bond is typically $\sim 3000 \text{ cm}^{-1}$ and is lowered to $\sim 2100 \text{ cm}^{-1}$ in C–D, the chemical reaction rate may decrease by a factor of up to ~ 6 depending on how prominently the C–H bond cleavage is featured in the transition state.⁴⁹ And indeed, incorporating deuterium into emitter molecules was reported to enhance the luminescence quantum yield, OLED efficiency and improve device lifetime, previously,^{50–53} but whether KIE can be used to stabilize the notoriously instable triplet blue emitters was not examined.

To better understand the KIE on the device performance, we first wished to establish a precise relationship between deuteration and the C–H/D activation. We constructed a computer model to identify the most vulnerable molecular sites and found that the benzylic C–H bonds are the weakest and most vulnerable C–H bonds. Thus, deuteration of the weakest benzylic C–H bond is expected to interrupt its bond cleavage and eventually the decomposition, giving rise to a more stable blue emitter. In order to verify this notion, we prepared various hydrogenated and deuterated homoleptic iridium complexes based on phenylimidazole ligands. The OLED devices were fabricated based on these eight iridium complexes. All complexes exhibit high external quantum efficiencies (EQEs) of 18.4–22.5% at 456–462 nm, and deuteration was found to significantly enhance the lifetime. In particular, the blue iridium complex **Ir1D** where the most vulnerable benzylic position was deuterated displayed an operational lifetime that was nearly doubled when compared to the protium-analogue to 355 hours (T_{70}) at 1000 cd/m^2 with high maximum EQE of 25.1% and good color purity (0.175, 0.285). To the best of our knowledge, this is the first case in which the instability of Ir-based blue emitters is overcome to such decisive extent by KIE, increasing the operational lifetime of blue OLEDs significantly. This finding also confirms the long-held suspicion that structural decomposition involving the activation of C–H bonds plays an important role in the deactivation of the blue dopant. The operational performances of the blue OLED device doped with **Ir1D** are one of the best among reported blue OLED devices. The novel device structures with the gradient doping in emission layer (EML) have shown to engender long device lifetime,^{26,64} but here we focus on a design of stable Ir-complexes embedded in a single stacked cell.

Results And Discussion

C–H Bond Strengths. To construct high-performing blue phosphorescent emitters, we first sought to identify the key factor that could affect the degradation of the device. Considering the observations from

previous studies mentioned above, it is clear that multiple factors contribute to the operational degradation of the emitter material with the most likely reactive components being the aromatic amines, carbazoles, hydrocarbons, and metal complexes.^{23,25,55–56} Whereas it is currently impossible to precisely identify the most disabling decomposition pathway, we can assess in more general terms the vulnerabilities that develop as the emitter molecule undergoes excitation. The triplet excited state in the Ir(III)-dopants are typically dominated by the metal-to-ligand-charge-transfer (MLCT) excitations, which can be formally envisioned as a reduction of the ligand. Among the many chemical reactions that this process may accelerate, we envisioned that the C–H activation and subsequent abstraction of hydrogen from the dopant is most likely. It is easy to imagine that the abstracted hydrogen atom can be transferred to an acceptor **[A⁺]**, as outlined in eqn 1, following an exciton-polaron annihilation mechanism, in which the hydrogen transfer from the excited triplet state of the dopant to a nearby receptor, e.g. the host material, takes place. The dehydrogenated Ir-dopant, which contains a carbon-centered radical, is likely to undergo further rearrangement and decomposition leading to unrecoverable loss of device performance.



To identify the C–H bond that is most vulnerable to such a transformation, we chose a series of homoleptic Ir-phenylimidazole emitters **Ir1–4** and calculated the adiabatic bond dissociation energies of all C–H bonds in the excited triplet state using density functional theory (DFT) calculations, as summarized in Table 1. To account for the screening environmental effect in the host material, a polarizable continuum solvation model was employed using a dielectric constant of toluene ($\epsilon = 2.38$). The computed C–H bond dissociation energies range from ~60 to as low as ~29 kcal/mol, with the benzylic C–H bonds showing the lowest bond dissociation energies. The benzylic C–H bonds in the ortho-positions (**3,10**) are calculated to require 31–28 kcal/mol in all Ir-complexes considered. The pyrimidyl (**1,2**) and phenylic (**4–7**) C–H bonds are also somewhat activated, but are unlikely to break at ~60 and ~50 kcal/mol, respectively. Given that the benzylic C–H bonds are also the weakest in ground state molecules with tabulated bond energies being ~90 kcal/mol compared to the phenylic bond being worth 113 kcal/mol, these calculated values are intuitively understandable. The calculated energy difference of the benzylic vs. phenylic C–H bonds of ~30 kcal/mol is also consistent with standard bond energies and indicate that all C–H bonds are activated by a similar amount in the MLCT state and the benzylic C–H bond becomes vulnerable simply because it is the weakest among the C–H bonds present in the phenyl-imidazole ligand.

Thus, the benzylic C–H bond is most vulnerable towards hydrogen abstraction, which may trigger the chemical decomposition of the device. DFT calculations were employed to estimate the barrier of the hydrogen abstraction reaction, where **Ir1** was chosen as a model. In these calculations, a cationic phenyl-carbazole moiety was used as the hydrogen atom acceptor, representing one possible acceptor functionality of a host-localized hole, as illustrated in Figure 1a. Our calculations show that the barrier of

the H-abstraction reaction is 23.7 kcal/mol, which is sufficiently low to take place even at mild conditions. The resulting benzyl radical and carbazolium species (**3**) were located at a relative energy of 21.5 kcal/mol, indicating the reaction is highly endergonic, and suggests that the transition state should be late and resemble the electronic structure of the product state according to the Hammond postulate.⁵⁷ As shown in Figure 1b, the benzylic hydrogen in the **TS** is located near the nitrogen with the length of C–H and N–H bonds being 1.52 and 1.19 Å, respectively.

To predict the effect of replacing C–H by C–D, we estimated the difference of the zero-point vibrational energy variation ($\Delta\Delta ZPE$) between **Ir1** and **Ir1'** where the benzylic hydrogen participating in the reaction was replaced by a deuterium. ΔZPE is the difference between the zero point vibrational energies at the TS and the reactant. The calculated $\Delta\Delta ZPE$ is 0.74 kcal/mol. Assuming Arrhenius-like dependence of the forward reaction rate on the barrier, the KIE can be estimated as:

$$KIE = \exp\left[\frac{\Delta\Delta ZPE}{kT}\right]$$

where k and T are the Boltzmann constant and temperature, respectively. At room temperature the KIE can be estimated to be 3.5 for **Ir1**, suggesting that the deuterated dopant would undergo the H-abstraction reaction notably slower than in the original dopant. Details of ZPE calculations are given in Table S1.

Taken together, these calculations highlight that the benzylic C–H bonds are potentially vulnerable functionalities and deuterating them may notably reduce the reaction rate of the dehydrogenation reaction. As predicted in the computational model, we sought to prepare a series of Ir-complexes with various degrees of deuterium incorporation and study the effect of the deuterium incorporation experimentally.

Synthesis and Characterization. The synthetic procedure for accessing **Ir1–4** and **Ir1D–4D** are shown in Figure 2. The ligands **L1–4** and **L1D–4D** were prepared using a palladium catalyzed cross coupling procedure.⁴⁰ Deuterium incorporation can be achieved by using deuterium oxide (D_2O) instead of water (H_2O) during the synthesis of **L1D–4D**. Ir(\square) complexes were prepared via a one-pot reaction of $Ir(COD)_2(BF_4)$ and the different ligands in a NMP (1-methyl-2-pyrrolidinone). All Ir(\square) complexes were purified by column chromatography and sublimation, and their structure were confirmed by 1H and ^{13}C NMR, MALDI-TOF and elemental analysis. All complexes are identified as facial structures by straightforward NMR spectra due to C_3 symmetry.⁵⁴ The total deuterium content of each complex is confirmed by 1H NMR and MALDI-TOF. Not surprisingly, the deuteration is not quantitative. Special attention was given to the degree of deuteration of the benzylic C–H bonds. Deuterium/protium ratios of **Ir1D–4D** were assigned by 1H NMR and quantified by comparing the integration of the corresponding NMR signals to an internal standard, the 5 or 6-position of the 3-cyanophenyl moiety that cannot be deuterated (Figures S1–S8).

Our experiments indicate that all methyl groups of **Ir1D–3D** are deuterated to ~90 %. The methyl and hydrogen of the isopropyl functionality in **Ir4D** show substitution levels of ~48 % and ~85 % and the hydrogen at the 4-position of the diisopropylphenyl of **Ir4D** is deuterated at ~74 %. The 2, 3-positions of the imidazole fragment in **Ir1D–4D** are confirmed to carry deuterium at ~69 % to 88 %. MALDI-TOF measurements of **Ir1D–4D** also show consistently that the molecular weight has increased by deuteration (Figure S9), fully consistent with the conclusions drawn from the NMR analysis.

Photophysical properties. With the Ir-complexes in hand, the photophysical properties were studied. As expected, **Ir1–4** and **Ir1D–4D** have practically identical absorption and emission spectra, and display the same electrochemical and thermal properties, as detailed in Table 2. The UV-vis absorption and photoluminescence (PL) spectra are shown in Figure 3. The absorption spectra of all compounds feature an intense absorption band at 260–330 nm that can be assigned to the spin-allowed π - π^* (LC) transition of the phenylimidazole ligand. The broad low-energy absorption band in the region of 360–450 nm is an admixture of the 1 MLCT and 3 MLCT transitions. When excited for emission at 360 nm, the emission spectra of all complexes in DCM solution show blue emission with maximum peaks displayed at 456–462 nm. The UV-vis edge of **Ir3** and **Ir3D** were blue-shifted by 0.3–0.4 eV and the PL were blue-shifted by 6 nm when compared to **Ir2** and **Ir2D** that do not contain the methyl substituent on the 3-cyanophenyl fragment. The UV-vis and PL spectrum of **Ir1–4** and deuterated **Ir1D–4D** iridium complexes are almost identical, confirming that the deuteration has a minimal impact on the photophysical properties.

The quantum yield (Φ) of all complexes measured in PMMA film employing the integrating sphere method were in the range of 0.94 to 0.99. Although it was reported previously that C-H vibrational oscillators suppressed by C-D replacement can enhance luminescent quantum efficiency and lifetime,^{58–59} we were unable to observe such a differential effect, presumably because the heavy transition metal overrides and minimizes the impact of the deuterium on the reduced mass relevant for the vibrations.⁵³ The emission lifetimes of 2.15–2.69 μ s for all complexes measured in PMMA film confirm the expected phosphorescence emission. The methyl functionality introduced in **Ir3** and **Ir3D** shift the excited state characteristics away from MLCT more towards the LC character, which results in reduced spin density on the iridium atom in the excited state and suppresses of the spin-orbit coupling between singlet and triplet manifolds, resulting in the decrease of the radiative decay rate compared to **Ir2** and **Ir2D** (Figure S14 and Table S2).

The HOMO and LUMO levels of the iridium complexes were determined by cyclic voltammetry and optical band gap (Table 1 and Figure S10). The HOMO energy levels were estimated from the onset of the oxidation potential and the LUMO energy levels were derived by adding the optical bandgaps to the HOMO energy levels. The HOMO for all complexes were in the range of –5.25 to –5.34 eV, and the adding the methyl groups to the 3-cyanophenyl moiety in **Ir3** and **Ir3D** gave rise to a shift of the HOMO/LUMO levels due to their electron-donating inductive nature. As the methyl groups are closer to the LUMO geometrically, the destabilizing effect is greater for the LUMO than the metal-centered HOMO, resulting in a greater HOMO-LUMO gap and a blue-shift of the emission. This finding is consistent with DFT calculations that showed a more pronounced blue-shift of **Ir3** and **Ir3D**. The thermal properties were

investigated by thermogravimetric analysis (TGA). The deposition temperatures at 5 % weight loss (T_{d5}) were found to be 415–475 °C (Figure S11), which is consistent with other phenylimidazole-based iridium complexes.

Device performances. To evaluate the effect of deuteration, OLED device were fabricated as follows: Indium tin oxide (ITO, 150nm) / p-doped (3wt%, NDP series, Novald AG) N-([1,10-biphenyl]-4-yl)-9,9-dimethyl-N-(4-(9-phenyl-9Hcarbazol-3-yl)phenyl)-9H-fluoren-2-amine (BCFA) (10nm) / BCFA(135nm) / H1(10nm) / H1:H2:Ir complexes (2,2'-di(9H-carbazol-9-yl)-1,1'-biphenyl (H1), 9-(3'-(9H-carbazol-9-yl)-5-cyano-[1,1'-biphenyl]-3-yl)-9Hcarbazole-3-carbonitrile (H2), 5:5:10%, 40nm) / mCP-CN(10nm) / codedped NET:NDN series, Novald AG (5:5, 30nm) / Al.⁶⁰⁻⁶¹

The Ir complexes **Ir1–4** and **Ir1D–4D** were studied in the same device structure and a detailed energy level diagram is shown in Figure 4a. A p-doped layer was used to achieve effective hole injection from ITO into hole transfer layer (HTL). For the enhancement of exciton confinement in the emission layer (EML), we employed the exciton and hole blocking layer (HBL) with high triplet energies (T_1 of H1: 3 eV, T_1 of HBL: 3.02eV). The EQE versus luminance, normalized electroluminescence (EL) spectra and lifetime curves ($LT_{70}@1000\text{cd/m}^2$) are plotted in Figures 4b–d. EML is composed of cohost system with H1 and H2 doped with the Ir complexes. H1 is the modified 3,3'-di(9H-carbazol-9-yl)-1,1'-biphenyl (mCBP) which has twisted structure by adopting ortho-likier bridge and can achieve higher triplet energy (3 eV) and higher hole mobility. H2 has the CN modified carbazole unit and biphenyl contributing to deep HOMO/LUMO levels and afford enhanced electron acceptor characteristics. H1 and H2 have effective HOMO/LUMO levels to enhance the hole and electron carrier injection, respectively, which improve the device performance. In particular, this cohost combination can form the stable exciplex at ~421 nm to efficiently support the triplet state of the Ir-dopant.⁶²

All OLED devices showed high efficiency and relatively long device lifetime at CIE < 0.3, and all relevant EL characteristics are summarized in Table 3. The devices incorporating **Ir1**, **Ir2** and **Ir4** show an EL emission at 462 nm, whereas **Ir3** displays slightly blue-shifted emission at 457 nm associated with a deep blue color characterized by CIE coordinates of (0.172, 0.258). **Ir1**, **Ir2** and **Ir4** show good device performance with EQE > 22 %, LT_{70} > 140 h. **Ir1** has the highest EQE of 22.5 % and a device lifetime LT_{70} of 182 hours, which may be attributed to the sterically bulky tert-butyl groups that inhibit intermolecular interaction that may lead to triplet-triplet annihilation.⁶³ The **Ir3** device shows the lowest device performance among the dopants tested. Because the HOMO levels are relatively shallow, holes are easily trapped in the **Ir3** devices and the operational voltage must be increased from ~4V to 4.5 V. Moreover, since the **Ir3** shows a blue-shifted emission peak, the energy transfer from cohost exciplex might not be sufficient. The **Ir3** device shows a relatively long decay time of ~2.69 μs and a roll-off increase of ~10 %, which is slightly higher than what is seen in the other dopants **Ir1** (7.9%), **Ir2** (5.4%), and **Ir4** (4.8%), resulting in the reduced EQE. Consequently, **Ir3** has device lifetime LT_{70} of ~51 hours at 1000cd/m² that is notably shorter than what is found with **Ir2** that exhibited a lifetime of over 140 hours, but the color of the emission was shifted to a deeper blue, indicated by CIE coordinates of (0.172, 0.258).

Not surprisingly, the EQE values of the **Ir1–4** and their deuterated analogues **Ir1D–4D** are almost identical, but the device lifetimes are dramatically enhanced by deuteration, confirming that inhibiting the C–H bond activation is a viable strategy for enhancing the lifetime of the OLED devices. Remarkably, the LT_{70} of **Ir1D**, **Ir2D**, and **Ir3D** doubled to 355, 290, and 92 hours, respectively, whereas the lifetime enhancement of **Ir4D** to 192 hours is relatively low due to the lower levels of methyl deuteration (48%) of the isopropyl group in **Ir4D**. Of particular interest is the observation that **Ir1D** displays highly efficient and stable device performance with a maximum EQE of 25.1 % and the LT_{70} being 355 hours emitting a deep blue color characterized by CIE coordinates of (0.175, 0.285) over high brightness of 1000cd/m². These device characteristics are found to be almost the best of the reported performances of blue phosphorescent materials.

To relate these KIE-based improvements of the lifetime to the calculated KIE mentioned above, we must account for the fact that deuterium incorporation was not quantitative, which will of course lower the experimentally observable KIE. To estimate the effective KIE_{eff} the fractional deuterium incorporation can be accounted for by:

$$KIE_{eff} = \frac{1}{(1-r) + r/KIE}$$

where r is typical deuteration ratio. The KIE_{eff} becomes 3 ± 0.2 for a deuteration ratio in the range of 85–90 % that was observed in Ir-complexes, which is in reasonably good agreement with the experimentally observed value ~ 2 .

Isothermal experiment was performed to confirm that the stability enhancement originates from increased stability of the deuterated dopants. The purity change of **Ir1–4** and **Ir1D–4D** after the isothermal process applying a constant temperature ~ 280 °C for 1 hour is shown in Table 4. The impurities of each hydrogenated and deuterated dopant have similar patterns, but in the case of the deuterated dopants, the purity change after the isothermal process is notably smaller compared to the undeuterated analogues. For example, **Ir3** has a purity change of 5.37% after being exposed to the isothermal conditions, but the deuterated analogue **Ir3D** shows a much improved behavior at 1.44%. The mass of major impurities was found to be oxidation products (see Figure S15), which is worrisome, as device degradation can be affected by oxidized material during electro- and photo-chemical processes.^{55,65} These isothermal experiments offer further support for the proposal that the durability of the Ir-dopants can be significantly enhanced by deuteration.

Conclusions

In this study, we demonstrate that KIE can significantly increase the operational lifetime of blue phosphorescent materials. We examined four homoleptic iridium(III)-complex carrying phenylimidazole ligands and their deuterated analogues to investigate whether the kinetic isotope effect can be employed to protect C–H bonds and extend the lifetime of deep blue emitters in phosphorescent OLED devices.

Computational studies were used to calculate the strengths of all C–H bonds in the triplet excited state, which indicated a substantial weakening of all C–H bonds due to repulsive nature of triplet state after its eventual localization on dissociating bond. The benzylic positions were identified as particularly vulnerable, and synthetic efforts were focused on deuterating these positions. The quantum yield (Φ) of all complexes measured in PMMA film with integrating sphere were excellent ranging from 0.94 to 0.99. Prototype OLED devices were constructed and all eight dopants exhibited blue emissions in the range of 456–462 nm. **Ir1D–4D** maintained high efficiency and device lifetime could be doubled when compared to **Ir1–4**, demonstrating that deuterium incorporation targeting the most vulnerable C–H bonds is a viable strategy to significantly increase the operational lifetime without introducing any change in chemical composition and altering the photophysical properties of the dopant. In particular, **Ir1D** showed one of the best device performances measured to date with a maximum EQE of 25.1% and a device lifetime of 355 hours (T_{70}) operating and 1000 cd/m² and displaying a deep blue color with color coordinates of (0.175, 0.285) on the CIE map. With the molecular mechanism of how the deuterium impacts the complex degradation, our studies that included isothermal stability experiments suggest that deuterium incorporation is an effective, non-invasive and supplementary tool that can be used in combination with other strategies for substantially enhancing the operational lifetime of phosphorescent OLED devices.

Methods

Device fabrication and measurements. All organic layers were deposited on patterned ITO glass using a thermal evaporation system with a vacuum pressure of $< 1.0 \cdot 10^{-7}$ torr after pre-cleaning of acetone, Isopropyl alcohol and deionized water sequentially. The common layers (HITL, EBL, HBL, ETL) and EML were deposited by 0.1 nm s^{-1} and 0.05 nm s^{-1} , respectively. The active area overlapped by the ITO anode and Al cathode was defined as 4mm^2 . The EL device structure was fabricated as follows; ITO / p doped BCFA / BCFA / H1 / H1:H2:Ir complexes / mCP-CN / ETL / Al. EL devices were encapsulated by the glass lid in high purity nitrogen glovebox. JVL characteristic including current, voltage was tested with a Keithley, 2400 Source-Meter and EL spectra and was collected by SR3 spectroradiometer. The operational lifetime of EL devices were measured in a constant current mode (designated current@1000nit and 0.2 mA/0.1 mA, respectively). Operation time where initial luminance was diminished to 70% is LT_{70} .

Computational Details. All calculations were performed using density functional theory (DFT) implemented in the Jaguar 9.1 suite of programs.⁶⁶ Geometries of all ground state (S_0) and the lowest triplet excited state (T_1) were optimized using PBE0⁶⁷ functional including Grimme's D3 dispersion^{68,69} correction with the 6-31G** basis set⁷⁰ for main group elements and the Los Alamos double-zeta basis^{71–73} containing effective core potentials for the transition metals. Single point calculations with Dunning's correlation-consistent triplet- ζ basis set, cc-pVTZ(-f)⁷⁴ were carried out to reevaluate the electronic energies. For iridium, LACV3P containing decontracted exponents to match the effective core potential with triple- ζ quality was used. The zero-point energy (ZPE) and entropy were obtained from the frequency calculations at the same level of theory used in the geometry optimization. For the evaluation

of vibrational entropy, low frequency vibrational modes below 50 cm^{-1} except the imaginary frequency in TS were replaced with a value of 50 cm^{-1} . Solvation energies were computed by a self-consistent reaction field (SCRF) approach⁷⁵⁻⁷⁷ with the dielectric constant $\epsilon = 2.379$ (toluene) using the gas phase optimized structures. All free energies (kcal/mol) in the energy profile in the manuscript were calculated at 298.15 K.

For the reactant state, the cationic acceptor and dopant (T_1 state) were treated as infinitely separated and since both components are immobilized in the device the translational entropy was eliminated when calculating the free energy. Therefore, the entropy corrections only consider the contributions from the vibrational and rotational degrees of freedom.

Declarations

Data availability

The authors declare that the all data supporting the findings of this study are available within the paper and the Supplementary Information files.

Competing financial interests

The authors declare no competing financial interests.

Author contribution

M.-H.B. and H.C. conceived and designed the project. H.J.B. and S.P. synthesized Ir(III) complexes. J.S.K. fabricated optical samples and devices. A.Y. and J.J. performed DFT calculations. J.C. and S.I. analyzed the data of material properties. W.-J.S. and Y.J. contributed to the interpretation of the computational and synthetic results, respectively. S.K. supervised the findings in device experiments.

Acknowledgements

This material is based upon work supported in part by the Samsung Advanced Institute of Technology (SAIT) and the Institute for Basic Science (IBS-R010-A1). We thank Seung-yeol Baek for providing helpful discussion (KAIST).

References

1. Adachi, C., Baldo, M. A., Thompson, M. E. & Forrest, S. R. Nearly 100% internal phosphorescence efficiency in an organic light-emitting device. *J. Appl. Phys.* **90**, 5048–5051 (2001).

- Baldo, M. A., Lamansky, S., Burrows, P. E., Thompson, M. E. & Forrest, S. R. Very high-efficiency green organic light-emitting devices based on electrophosphorescence. *Appl. Phys. Lett.* **75**, 4–6 (1999).
- Baldo, M. A. *et al.* Highly efficient phosphorescent emission from organic electroluminescent devices. *Nature* **395**, 151–154 (1998).
- Wong, W.-Y. *et al.*, Multifunctional iridium complexes based on carbazole modules as highly efficient electrophosphors. *Angew. Chem., Int. Ed.* **45**, 7800–7803 (2006).
- Lee, C.-L., Lee, K. B. & Kim, J.-J. Polymer phosphorescent light-emitting devices doped with tris(2-phenylpyridine) iridium as a triplet emitter. *Appl. Phys. Lett.* **77**, 2280–2282 (2000).
- Lamansky, S. *et al.* Highly phosphorescent bis-cyclometalated iridium complexes: Synthesis, photophysical characterization, and use in organic light emitting diodes. *J. Am. Chem. Soc.* **123**, 4304–4312 (2001).
- Lamansky, S. *et al.* Synthesis and characterization of phosphorescent cyclometalated iridium complexes. *Inorg. Chem.* **40**, 1704–1711 (2001).
- Chen, Z.-Q., Bian, Z.-Q. & Huang, C.-H. Functional Ir^{III} complexes and their applications. *Adv. Mater.* **22**, 1534–1539 (2010).
- Coppo, P., Plummer, E. A. & De Cola, L. Tuning iridium(III) phenylpyridine complexes in the “almost blue” region. *Chem. Commun.*, 1774–1775 (2004)
- Lu, K.-Y. *et al.* Wide-range color tuning of iridium biscarbene complexes from blue to red by different *N^N* Ligands: an Alternative route for adjusting the emission colors. *Adv. Mater.* **23**, 4933–4937 (2011).
- Tsuboyama, A. *et al.* Homoleptic cyclometalated iridium complexes with highly efficient red phosphorescence and application to organic light-emitting diode. *J. Am. Chem. Soc.* **125**, 12971–12979 (2003).
- You, Y. & Park, S. Y. Phosphorescent iridium(III) complexes: Toward high phosphorescence quantum efficiency through ligand control. *Dalton Trans.*, 1267–1282 (2009).
- Li, T. Y. *et al.* Rational design of phosphorescent iridium(III) complexes for emission color tunability and their applications in OLEDs. *Coord. Chem. Rev.* **374**, 55–92 (2018).
- Feng, Z., Sun, Y., Yang, X. & Zhou, G. Novel emission color-tuning strategies in heteroleptic phosphorescent Ir(III) and Pt(II) complexes. *Chem. Rec.* **19**, 1710–1728 (2019).
- Grushin, V. V. *et al.* New, efficient electroluminescent materials based on organometallic Ir complexes. *Chem. Commun.*, 1494–1495 (2001).
- Tsuzuki, T., Shirasawa, N., Suzuki, T. & Tokito, S. Color tunable organic light-emitting diodes using pentafluorophenyl-substituted iridium complexes. *Adv. Mater.* **15**, 1455–1458 (2003).
- Urinda, S., Das, G., Pramanik, A. & Sarkar, P. Quantum chemical investigation on the Ir(III) complexes with an isomeric triazine-based imidazolium carbene ligand for efficient blue OLEDs. *Phys. Chem. Chem. Phys.* **19**, 29629–29640 (2017).

18. Jacquemin, D. & Escudero, D. The short device lifetimes of blue PhOLEDs: insights into the photostability of blue Ir(III) complexes. *Chem. Sci.* **8**, 7844–7850 (2017).
19. Yang, X., Zhou, G. & Wong, W.-Y. Functionalization of phosphorescent emitters and their host materials by main-group elements for phosphorescent organic light-emitting devices. *Chem. Soc. Rev.* **44**, 8484–8475 (2015).
20. Lee, J.-H. *et al.* Blue organic light-emitting diodes: Current status, challenges, and future outlook. *J. Mater. Chem. C* **7**, 5874–5888 (2019).
21. Yang, X., Xu, X. & Zhou, G. Recent advances of the emitters for high performance deep-blue organic light-emitting diodes. *J. Mater. Chem. C* **3**, 913–944 (2015).
22. Ho, C.-L. & Wong, W. Y. Small-molecular blue phosphorescent dyes for organic light-emitting devices. *New J. Chem.* **37**, 1665–1683 (2013).
23. Kim, S. *et al.* Degradation of blue-phosphorescent organic light-emitting devices involves exciton-induced generation of polaron pair within emitting layers. *Nat. Commun.* **9**, 1211 (2018).
24. Song, W. & Lee, J. Y. Degradation mechanism and lifetime improvement strategy for blue phosphorescent organic light-emitting diodes. *Adv. Opt. Mater.* **5**, 1600901 (2017).
25. Schmidbauer, S., Hohenleutner, A. & König, B. Chemical degradation in organic light-emitting devices: Mechanisms and implications for the design of new materials. *Adv. Mater.* **25**, 2114–2129 (2013).
26. Zhang, Y., Lee, J. & Forrest, S. R. Tenfold increase in the lifetime of blue phosphorescent organic light-emitting diodes. *Nat. Commun.* **5**, 5008 (2014).
27. Giebink, N. C. *et al.* Intrinsic luminance loss in phosphorescent small-molecule organic light emitting devices due to bimolecular annihilation reactions. *J. Appl. Phys.* **103**, 044509 (2008).
28. Han, L., Zhang, D., Wang, J., Lan, Z. & Yang, R. Efficiency phosphorescent OLEDs with a low roll-off based on a hetero-triplet iridium complex. *Dyes Pigm.* **113**, 649–654 (2015).
29. Murawski, C., Leo, K. & Gather, M. C. Efficiency roll-off in organic light-emitting diodes. *Adv. Mater.* **25**, 6801–6827 (2013).
30. Reineke, S., Schwartz, G., Walzer, K., Falke, M. & Leo, K. Highly phosphorescent organic mixed films: The effect of aggregation on triplet-triplet annihilation. *Appl. Phys. Lett.* **94**, 163305 (2009).
31. Xiang, C. Y. *et al.* Efficiency roll-off in blue emitting phosphorescent organic light emitting diodes with carbazole host materials. *Adv. Funct. Mater.* **26**, 1463–1469 (2016).
32. Adachi, C. *et al.* Endothermic energy transfer: A mechanism for generating very efficient high-energy phosphorescent emission in organic materials. *Appl. Phys. Lett.* **79**, 2082–2084 (2001).
33. Shin, H. Sky-blue phosphorescent OLEDs with 34.1% external quantum efficiency using a low refractive index electron transporting layer. *Adv. Mater.* **28**, 4920–4925 (2016).
34. Baranoff, E. D. & Curchod, B. Flrpic: archetypal blue phosphorescent emitter for electroluminescence. *Dalton Trans.* **44**, 8318–8329 (2015).
35. de Moraes, I. R., Scholz, S., Lüssem, B. & Leo, K. Analysis of chemical degradation mechanism within sky blue phosphorescent organic light emitting diodes by laser-desorption/ionization time-of-flight

- mass spectrometry. *Org. Electron.*, **12**, 341–347 (2011).
36. Seifert, R. *et al.* Chemical degradation mechanisms of highly efficient bluephosphorescent emitters used for organic light emitting diodes. *Org. Electron.* **14**, 115–123 (2013).
 37. Sivasubramaniam, V. *et al.* Fluorine cleavage of the light blue heteroleptic triplet emitter Flrpic. *J. Fluor. Chem.* **130**, 640–649 (2009).
 38. Baranoff, E. *et al.* Acid-induced degradation of phosphorescent dopants for OLEDs and its application to the synthesis of tris-heteroleptic iridium(III) bis-cyclometalated complexes. *Inorg. Chem.* **51**, 215–224 (2012).
 39. Zhuang, J. Homoleptic tris-cyclometalated iridium(III) complexes with phenylimidazole ligands for highly efficient sky-blue OLEDs. *New J. Chem.* **39**, 246–253 (2015).
 40. Kwon, Y., Han, S. H., Yu, S., Lee, J. Y. & Lee, K. M. Functionalized phenylimidazole-based facial-homoleptic iridium(III) complexes and their excellent performance in blue phosphorescent organic light-emitting diodes. *J. Mater. Chem. C* **6**, 4565–4572 (2018).
 41. Udagawa, K., Sasabe, H., Cai, C. & Kido, J. Low-driving-voltage blue phosphorescent organic light emitting devices with external quantum Efficiency of 30%. *Adv. Mater.* **26**, 5062–5066 (2014).
 42. Zhuang, J. *et al.* Highly efficient phosphorescent organic light-emitting diodes using a homoleptic iridium(III) complex as a sky-blue dopant. *Org. Electron.* **14**, 2596–2601 (2013).
 43. Lee, J. *et al.* Deep blue phosphorescent organic light-emitting diodes with very high brightness and efficiency. *Nat. Mater.* **15**, 92–98 (2016).
 44. Schrögel, P. *et al.* Meta-linked CBP-derivatives as host materials for a blue iridiumcarbene complex. *Org. Electron.* **12**, 2047–2055 (2011).
 45. Sasabe, H. *et al.* High-efficiency blue and white organic light-emitting devices incorporating a blue iridium carbene complex. *Adv. Mater.* **22**, 5003–5007 (2010).
 46. Chang, C.-H. *et al.* A new class of sky-blue-emitting Ir(III) phosphors assembled using fluorine-free pyridyl pyrimidine cyclometalates: Application toward high-performance sky-blue- and white-emitting OLEDs. *ACS Appl. Mater. Interfaces* **5**, 7341–7351 (2013).
 47. Shin, H. Y., Jeong, S., Kim, S. H. & Hong, J.-I. Blue phosphorescent iridium complexes with fluorine-free main ligands for efficient organic light-emitting diodes. *Bull. Korean Chem. Soc.* **38**, 830–837 (2017).
 48. Anslyn, E. V. & Dougherty, D. A. *Modern Physical Organic Chemistry* (University Science Books, 2006)
 49. Jarczewski, A. & Hubbard, C. D. A review of proton transfer reactions between various carbon-acids and amine bases in aprotic solvents. *J. Mol. Struct.* **649**, 287–307 (2003).
 50. Tong, C. C. & Hwang, K. C. Enhancement of OLED efficiencies and high-voltage stabilities of light-emitting materials by deuteration. *J. Phys. Chem. C* **111**, 3490–3494 (2007).
 51. Tsuji, H., Mitsui, C. & Nakamura, E. The hydrogen/deuterium isotope effect of the host material on the lifetime of organic light-emitting diodes. *Chem. Commun.* **50**, 14870–14872 (2014).

52. Abe, T., Miyazawa, A., Konno, H. & Kawanishi, Y. Deuteration isotope effect on nonradiative transition of *fac*-tris(2-phenylpyridinato) iridium (III) complexes. *Chem. Phys. Lett.* **491**, 199–202 (2010).
53. Wang, P. *et al.* Synthesis of all-deuterated tris(2-phenylpyridine) iridium for highly stable electrophosphorescence: The “deuterium effect”. *J. Mater. Chem. C* **1**, 4821–4825 (2013).
54. Tamayo, A. B. *et al.* Synthesis and characterization of facial and meridional tris-cyclometalated iridium(III) complexes. *J. Am. Chem. Soc.* **125**, 7377–7387 (2003).
55. Scholz, S., Kondakov, D., Lüssem, B. & Leo, K. Degradation mechanisms and reactions in organic light-emitting devices. *Chem. Rev.* **115**, 8449–8503 (2015).
56. So, F. & Kondakov, D. Degradation mechanisms in small-molecule and polymer organic light-emitting diodes. *Adv. Mater.* **22**, 3762–3777 (2010).
57. Carey, F. & Sundberg, R. *Advanced Organic Chemistry Part A: Structure and Mechanisms* (Springer, 2007)
58. Doffek, C. *et al.* Understanding the Quenching Effects of Aromatic C – H- and C – DOscillators in Near-IR Lanthanoid Luminescence. *J. Am. Chem. Soc.* **134**, 16413–16423 (2012).
59. Hasegawa, Y. *et al.* Enhanced emission of deuterated tris(hexafluoroacetylacetonato)neodymium(III) complex in solution by suppression of radiationless transition via vibrational excitation. *J. Phys. Chem.* **100**, 10201–10205 (1996).
60. Hong, S., Kim, J. W. & Lee, S. Lifetime enhanced phosphorescent organic light emitting diode using an electron scavenger layer. *Appl. Phys. Lett.* **107**, 04117 (2015).
61. Lee, S. *et al.*, The role of charge balance and excited state levels on device performance of exciplex-based phosphorescent organic light emitting diodes. *Scientific reports* **7**, 11995, (2017).
62. Shin, S. K., Han, S. H. & Lee, J. Y. High triplet energy exciplex host derived from a CN modified carbazole based n-type host for improved efficiency and lifetime in blue phosphorescent organic light-emitting diodes. *J. Mater. Chem. C* **6**, 10308–10314 (2018)
63. Wen, L.-L. *et al.* Low efficiency roll-off and high performance OLEDs employing alkyl group modified iridium(III) complexes as emitters. *RSC Adv.* **6**, 111556–111563 (2016).
64. Klimes, K., Zhu, Z. Q. & Li, J. Efficient blue phosphorescent OLEDs with improved stability and color purity through judicious triplet exciton management. *Adv. Funct. Mater.* **29**, 1903068 (2019).
65. Cui, L.-S. *et al.* Controlling Synergistic Oxidation Processes for Efficient and Stable Blue Thermally Activated Delayed Fluorescence Devices. *Adv. Mater.* **28**, 7620–7625 (2016).
66. Bochevarov, A. D. *et al.* Jaguar: A High-Performance Quantum Chemistry Software Program with Strengths in Life and Materials Sciences. *Int. J. Quantum Chem.* **113**, 2110–2142 (2013).
67. Adamo, C. & Barone, V. Toward reliable density functional methods without adjustable parameters: The PBE0 model. *J. Chem. Phys.* **110**, 6158–6170 (1999).
68. Grimme, S. Semiempirical GGA-type density functional constructed with a long-range dispersion correction. *J. Comput. Chem.* **27**, 1787–1799 (2006).

69. Grimme, S., Antony, J., Ehrlich, S. & Krieg, H. A consistent and accurate ab initio parametrization of density functional dispersion correction (DFT-D) for the 94 elements H-Pu. *J. Chem. Phys.* **132**, 154104–154119 (2010).
70. R., Hehre, Ditchfield, W. J. & Pople, J. A. Self-consistent molecular-orbital methods. XII. Further extensions of Gaussian-type basis sets for use in molecular orbital studies of organic molecules. *J. Chem. Phys.* **56**, 2257–2261 (1972).
71. Hay, P. J. & Wadt, W. R. *Ab initio* effective core potentials for molecular calculations. Potentials for the transition metal atoms Sc to Hg. *J. Chem. Phys.* **82**, 270–283 (1985).
72. Hay, P. J. & Wadt, W. R. *Ab initio* effective core potentials for molecular calculations. Potentials for main group elements Na to Bi. *J. Chem. Phys.* **82**, 284–298 (1985).
73. Hay, P. J. & Wadt, W. R. *Ab initio* effective core potentials for molecular calculations. Potentials for K to Au including the outermost core orbitals. *J. Chem. Phys.* **82**, 299–310 (1985).
74. Dunning, T. H. Jr. Gaussian basis sets for use in correlated molecular calculations. I. The atoms boron through neon and hydrogen. *J. Chem. Phys.* **90**, 1007–1023 (1989).
75. Marten, B. *et al.* New model for calculation of solvation free energies: Correction of self-consistent reaction field continuum dielectric theory for short-range hydrogen-bonding effects. *J. Phys. Chem.* **100**, 11775–11788 (1996).
76. Edinger, S. R., Cortis, C., Shenkin, P. S. & Friesner, R. A. Solvation free energies of peptides: comparison of approximate continuum solvation models with accurate solution of the Poisson-Boltzmann equation. *J. Phys. Chem. B* **101**, 1190–1197 (1997).
77. Friedrichs, M., Zhou, R. H., Edinger, S. R. & Friesner, R. A. Poisson-Boltzmann analytical gradients for molecular modeling calculations. *J. Phys. Chem. B* **103**, 3057–3061 (1999).

Tables

Table 1. Bond dissociation energies of Ir1–4 complexes.

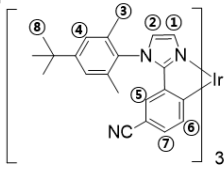
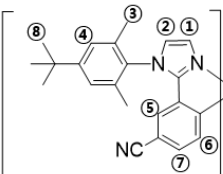
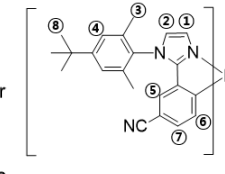
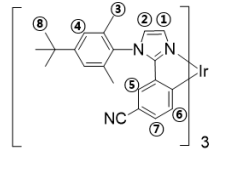
Bond dissociation energy for dopants in T ₁ state in kcal/mol				
	Ir1	Ir2	Ir3	Ir4
Bond number				
1	60.9	59.6	59.4	60.4
2	62.1	62.0	61.0	62.1
3	30.5	30.6	30.0	28.3
4	51.5	53.3	52.1	52.5
5	51.0	52.5	51.2	53.0
6	50.4	50.5	49.8	51.2
7	52.1	52.1	-	52.4
8	42.9	-	-	-
9	-	30.3	29.7	-
10	-	-	28.8	-
11	-	-	-	42.7
12	-	-	-	52.6

Table 2. Summarized photophysical properties of Ir1-4 and Ir1D-4D.

	$\lambda_{\text{abs}}^{\text{a}}$ (nm)	$\lambda_{\text{em}}^{\text{b}}$ (nm)	$\eta_{\text{film}}^{\text{c}}$	$\tau_{\text{film}}^{\text{c}}$ (μs)	HOMO ^d (eV)	LUMO ^e (eV)	T _{d5} (°C)	E _g ^f (eV)
Ir1	266, 322, 373, 404	462	0.94	2.15	-5.33	-2.31	4413.02	
Ir2	267, 322, 373, 404	462	0.96	2.18	-5.32	-2.30	4673.02	
Ir3	269, 321, 369, 401	456	0.97	2.69	-5.25	-2.20	4733.05	
Ir4	266, 322, 374, 405	462	0.94	2.17	-5.34	-2.34	4183.00	
Ir1D	266, 323, 373, 404	461	0.97	2.15	-5.32	-2.29	4413.02	
Ir2D	267, 321, 373, 404	462	0.97	2.15	-5.31	-2.29	4553.02	
Ir3D	268, 320, 370, 401	456	0.96	2.68	-5.26	-2.20	4753.06	
Ir4D	266, 323, 374, 405	462	0.99	2.18	-5.34	-2.31	4153.00	

^aMeasured in CH₂Cl₂ at 298 K in (1 × 10⁻⁵ M). ^bMeasured in CH₂Cl₂ at 298K in (1 × 10⁻⁴ M).

^c0.5 wt% doped film in PMMA. ^dMeasured from cyclic voltammetry scanning.

^eLUMO = HOMO + E_g. ^dThe optical band gap calculated from the absorption spectra.

Table 3. Summary of device performance

dopant	λ_{EL} (nm)	Op. V ^{a)} (V)	EQE ^{b)} (%)	Max. EQE (%)	LT ₇₀ (hrs)	Roll-off (%)	CIE ^{c)}
Ir1	462	4.09	22.5	24.8	182	7.9	(0.175, 0.285)
Ir2	462	4.02	21.6	23.1	140	5.4	(0.175, 0.283)
Ir3	457	4.52	18.6	21.0	51	10.1	(0.172, 0.258)
Ir4	462	3.75	22.1	23.2	154	4.8	(0.173, 0.280)
Ir1D	462	4.08	22.5	25.1	355	8.7	(0.175, 0.285)
Ir2D	462	4.02	21.8	23.7	290	6.6	(0.174, 0.284)
Ir3D	457	4.51	18.4	21.0	92	10.5	(0.171, 0.255)
Ir4D	462	3.80	22.1	23.3	192	5.1	(0.174, 0.280)

a) operational voltage, b) external quantum efficiency, c) 1931 Commission Internationale de L'Eclairage

Table 4. The purity of Ir1-4 and Ir1D-4D before and after isothermal process

	Ir1	Ir2	Ir3	Ir4	Ir1D	Ir2D	Ir3D	Ir4D
Before isothermal	99.82%	99.70%	99.99%	99.00%	99.82%	99.97%	99.87%	98.76%
After ^{a)} isothermal	99.38%	96.49%	94.62%	98.75%	99.63%	98.80%	98.43%	98.55%

a) isothermal process condition: ~280 °C (average sublimation temperature of dopants), 1 hr, air.

Figures

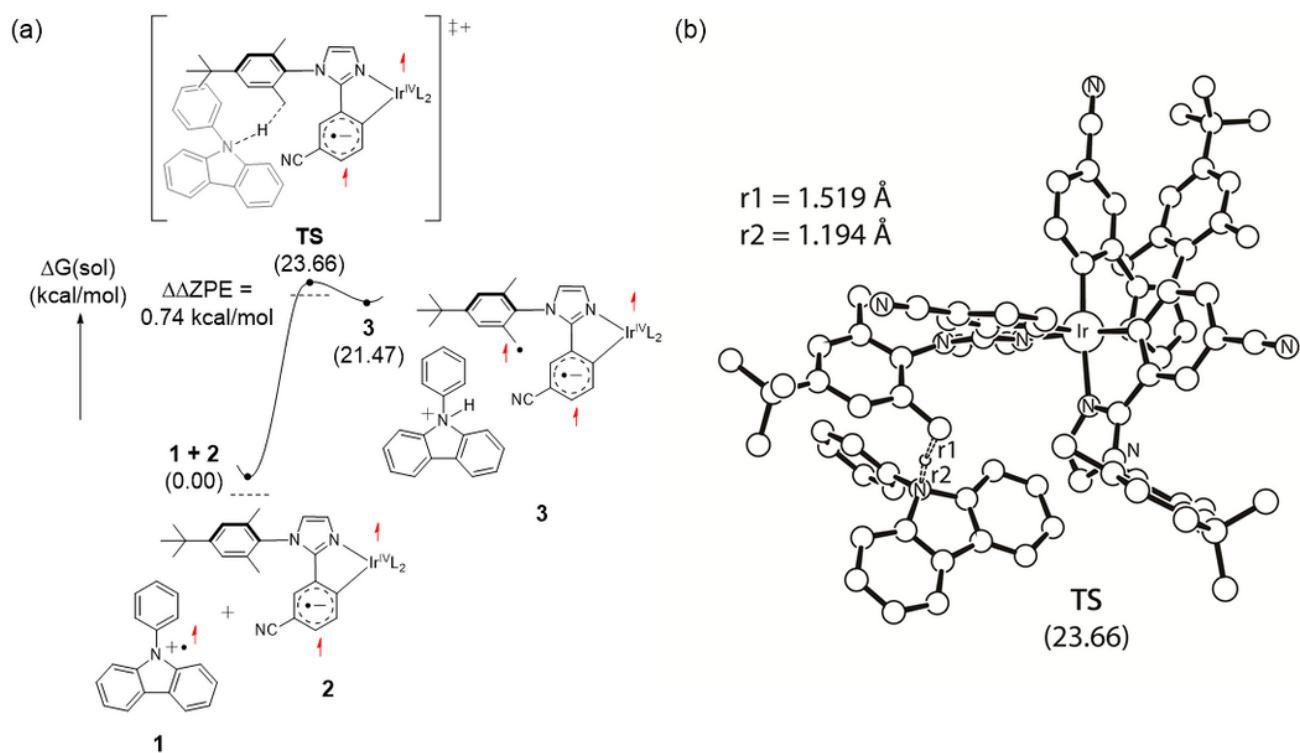


Figure 1

(a) Hydrogen transfer reaction trajectory from Ir1 in the lowest triplet excited state to phenyl-carbazole in the cationic state. (b) The optimized structure of the transition state of hydrogen abstraction reaction (TS).

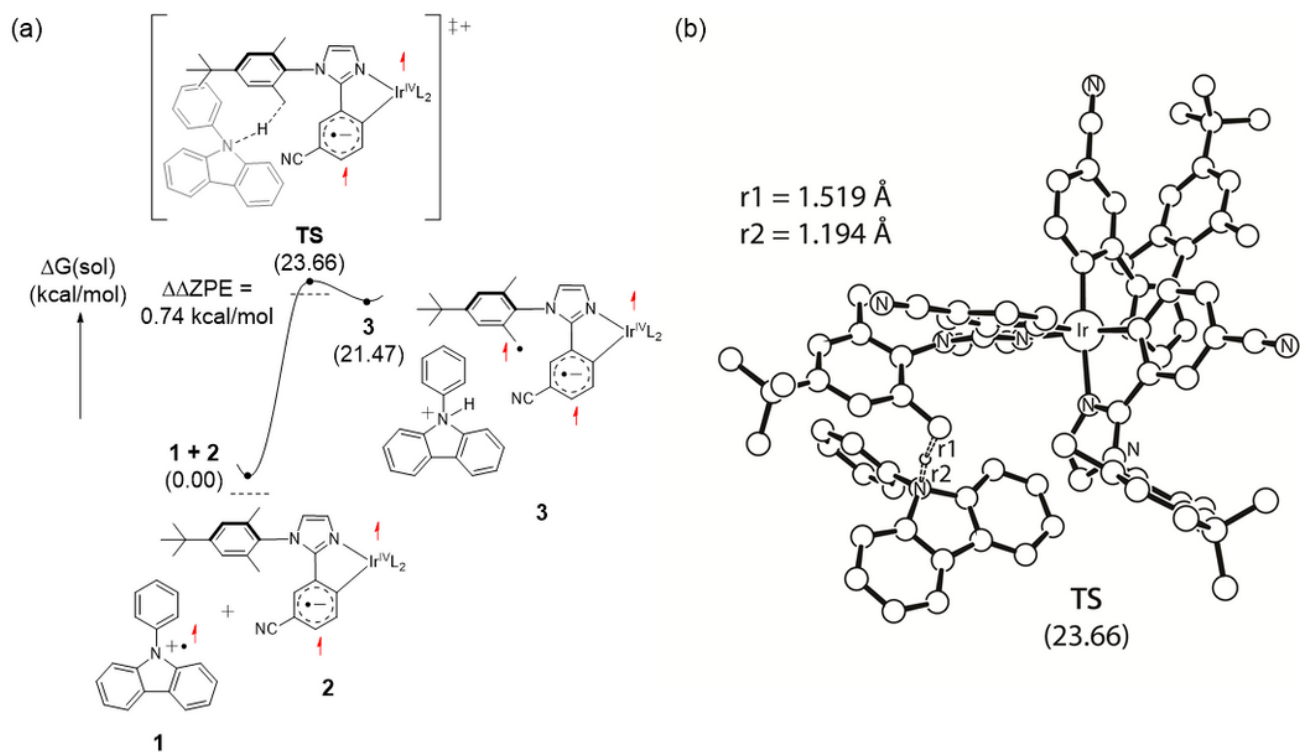


Figure 1

(a) Hydrogen transfer reaction trajectory from Ir1 in the lowest triplet excited state to phenyl-carbazole in the cationic state. (b) The optimized structure of the transition state of hydrogen abstraction reaction (TS).

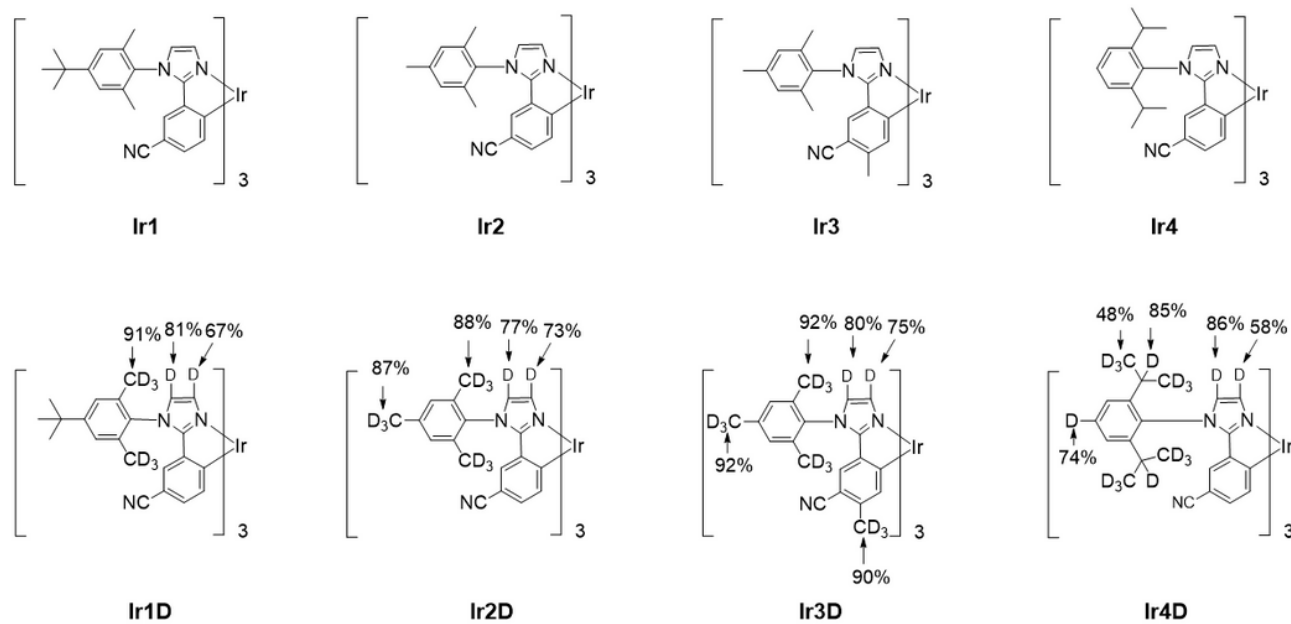
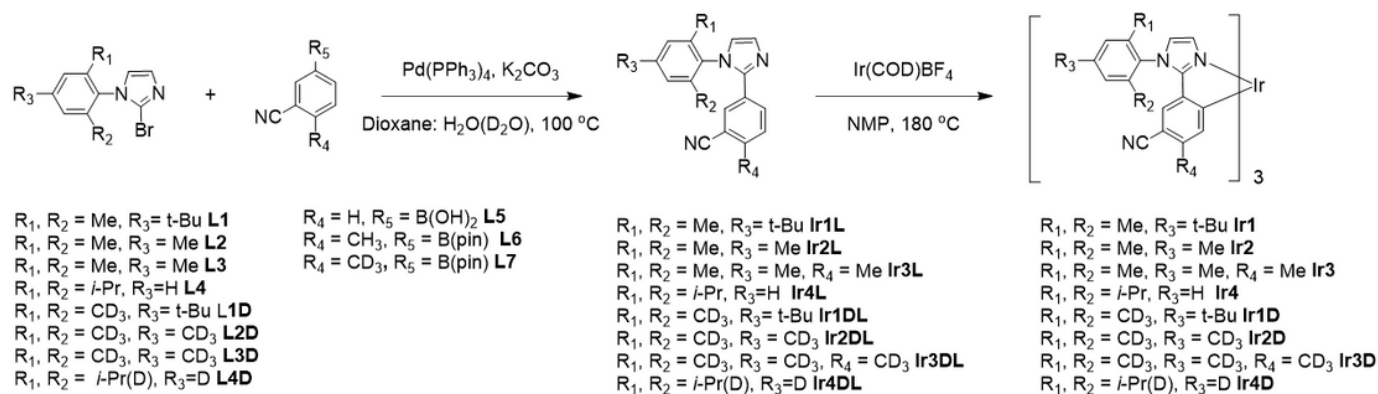


Figure 2

Synthetic route of materials and structures.

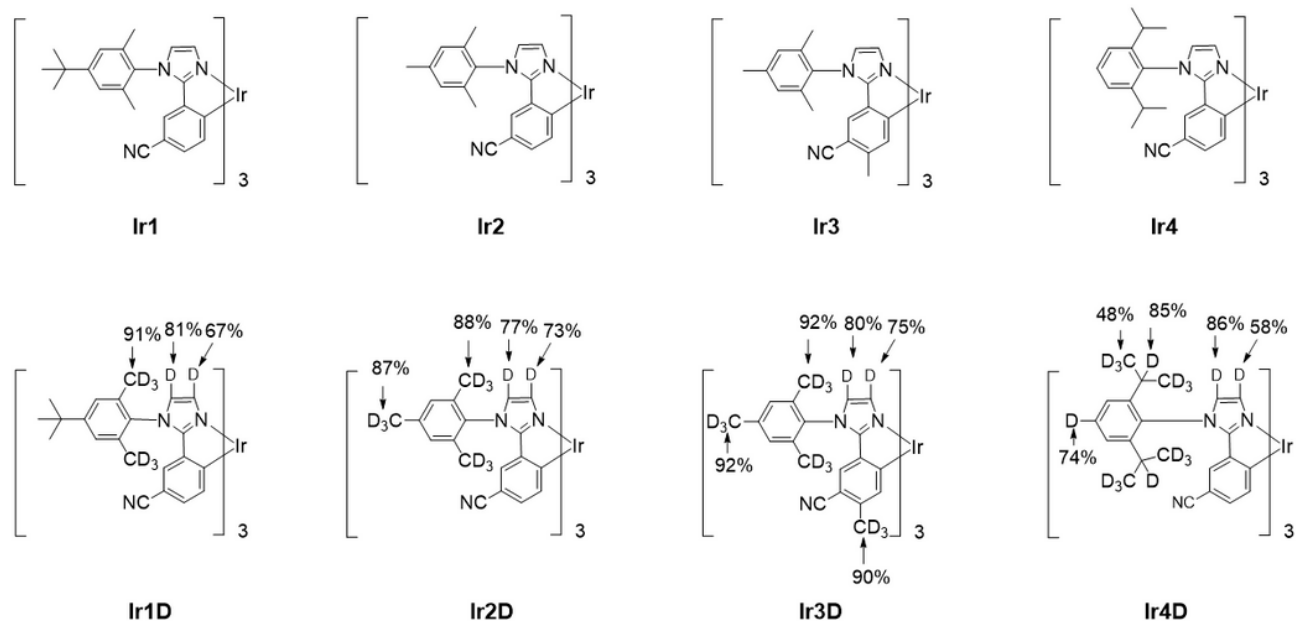
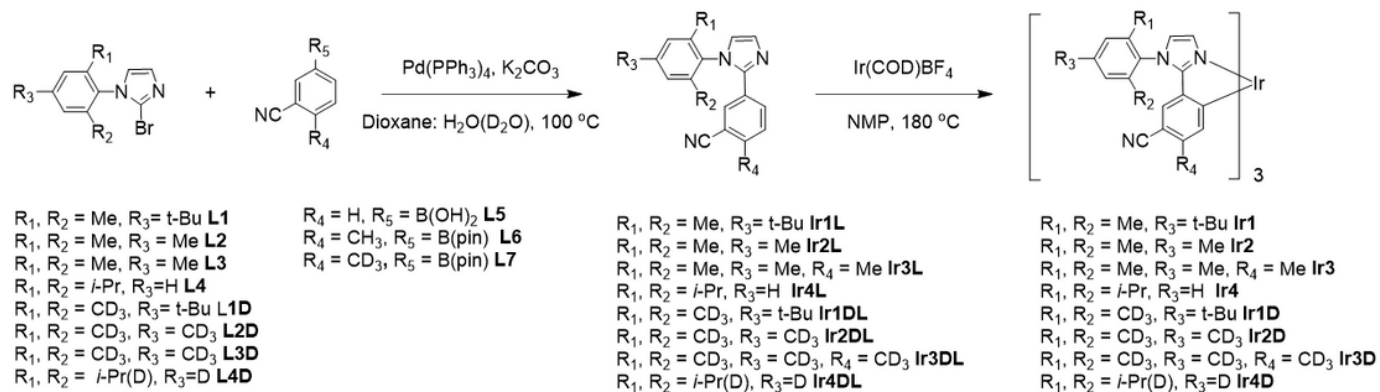


Figure 2

Synthetic route of materials and structures.

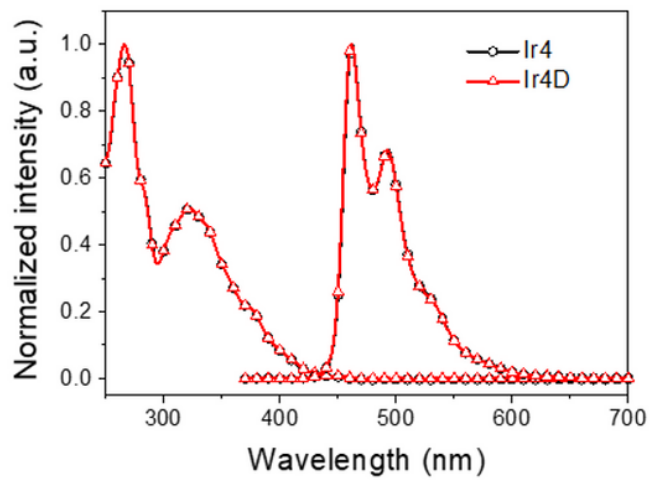
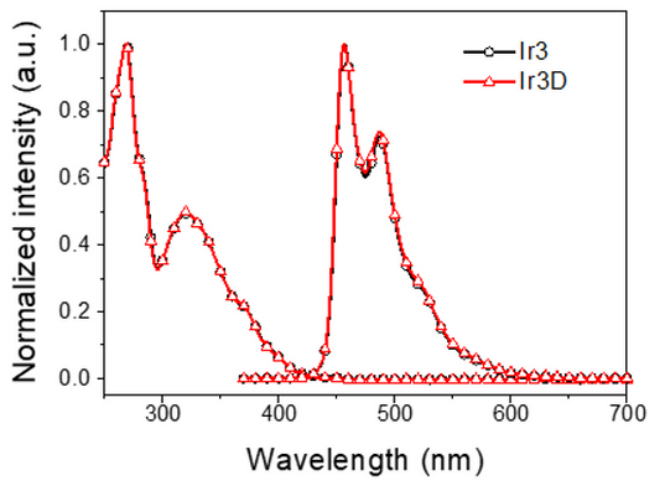
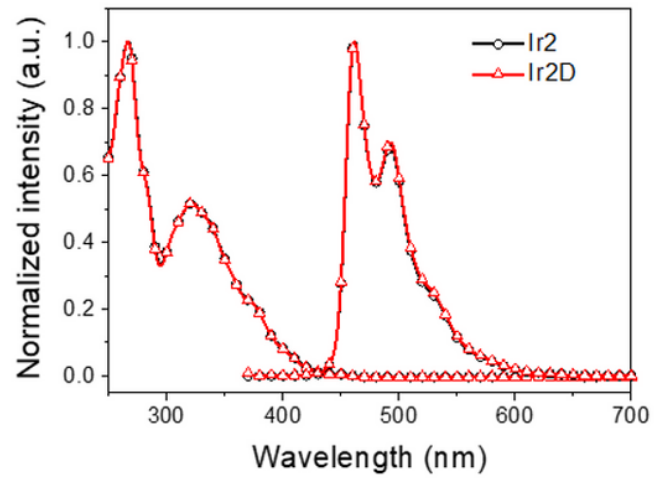
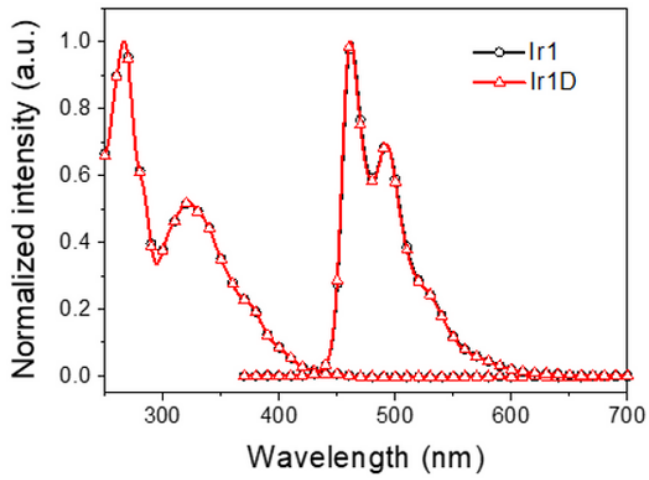


Figure 3

UV-vis and PL spectra of (a) Ir1-1D, (b) Ir2-2D, (c) Ir3-3D and Ir4-4D.

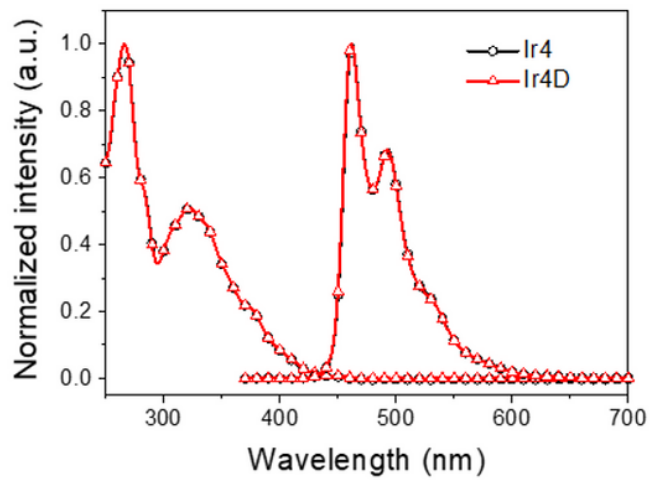
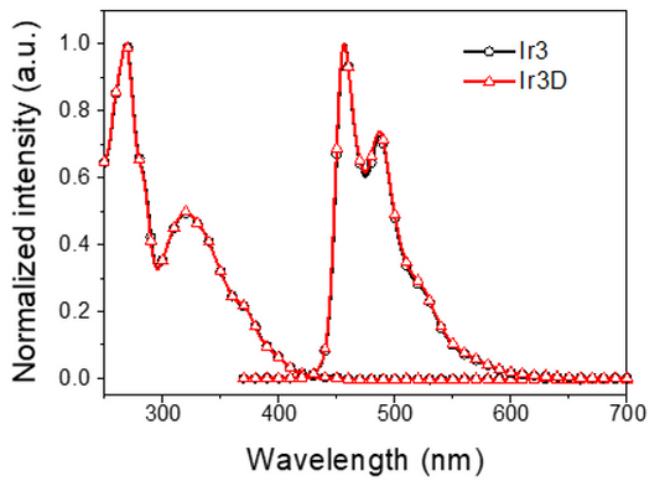
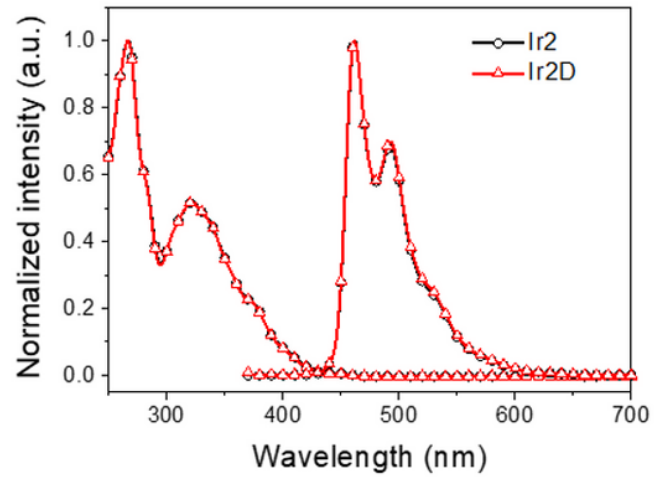
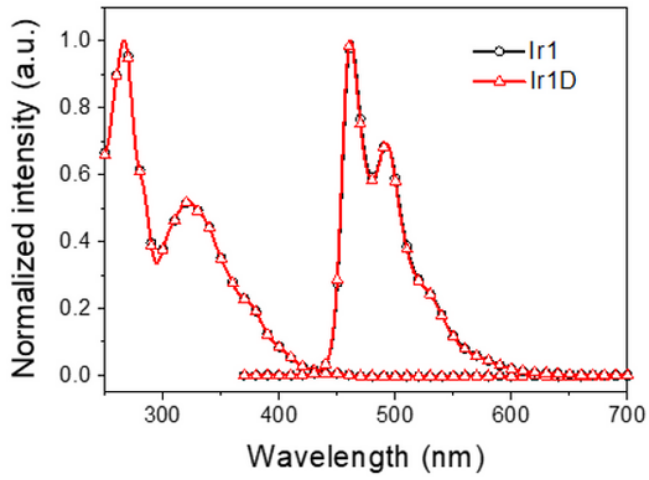


Figure 3

UV-vis and PL spectra of (a) Ir1-1D, (b) Ir2-2D, (c) Ir3-3D and Ir4-4D.

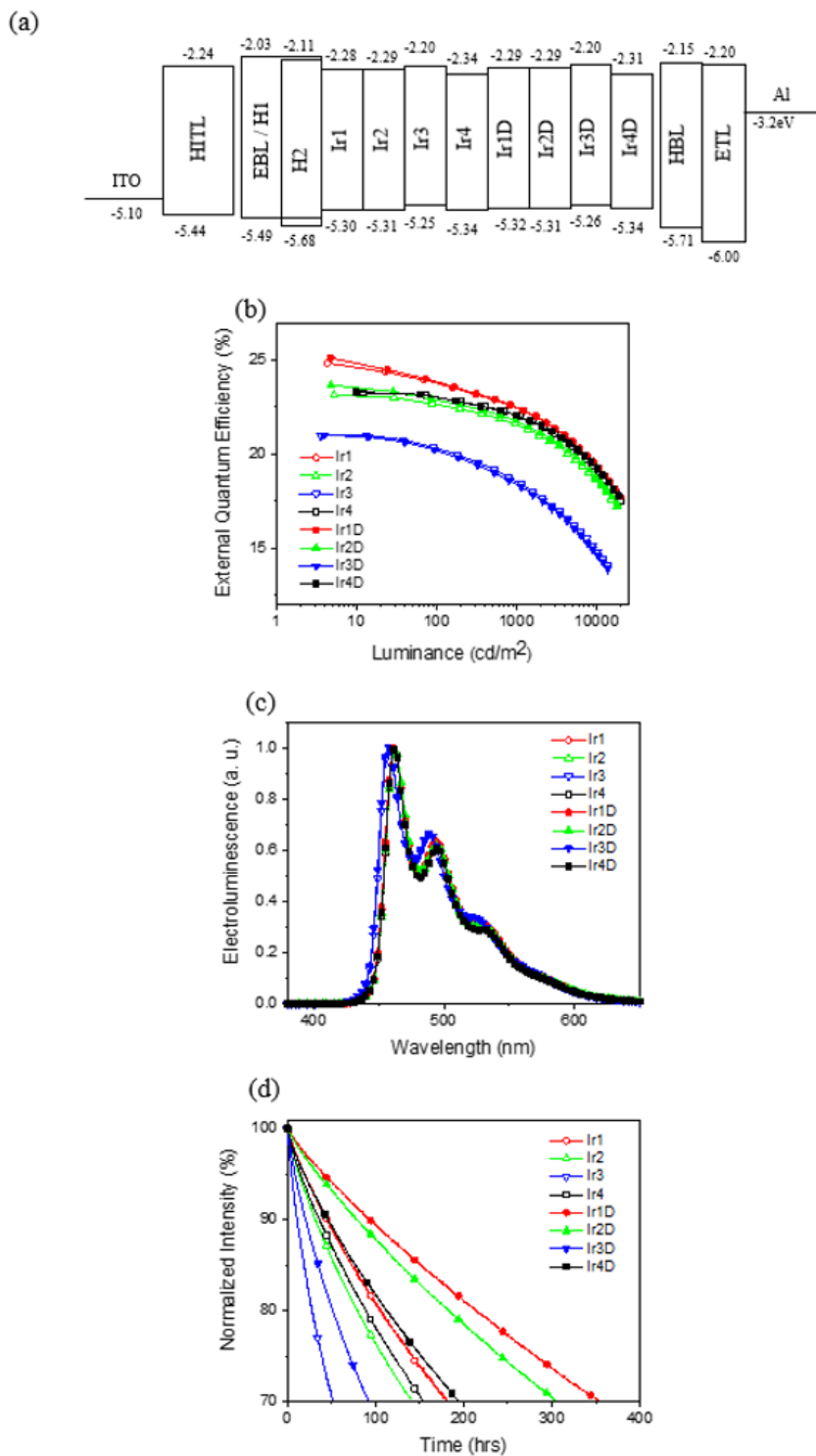


Figure 4

Device performances. (a) Energy level diagram of optimized device structures (unit of energy: eV), (b) external quantum efficiency as a function of luminance(cd/m^2), (c) normalized electroluminescence spectra and (d) normalized EL intensity vs. operational life time at $1000 \text{ cd}/\text{m}^2$ for each Ir complexes doped OLED devices.

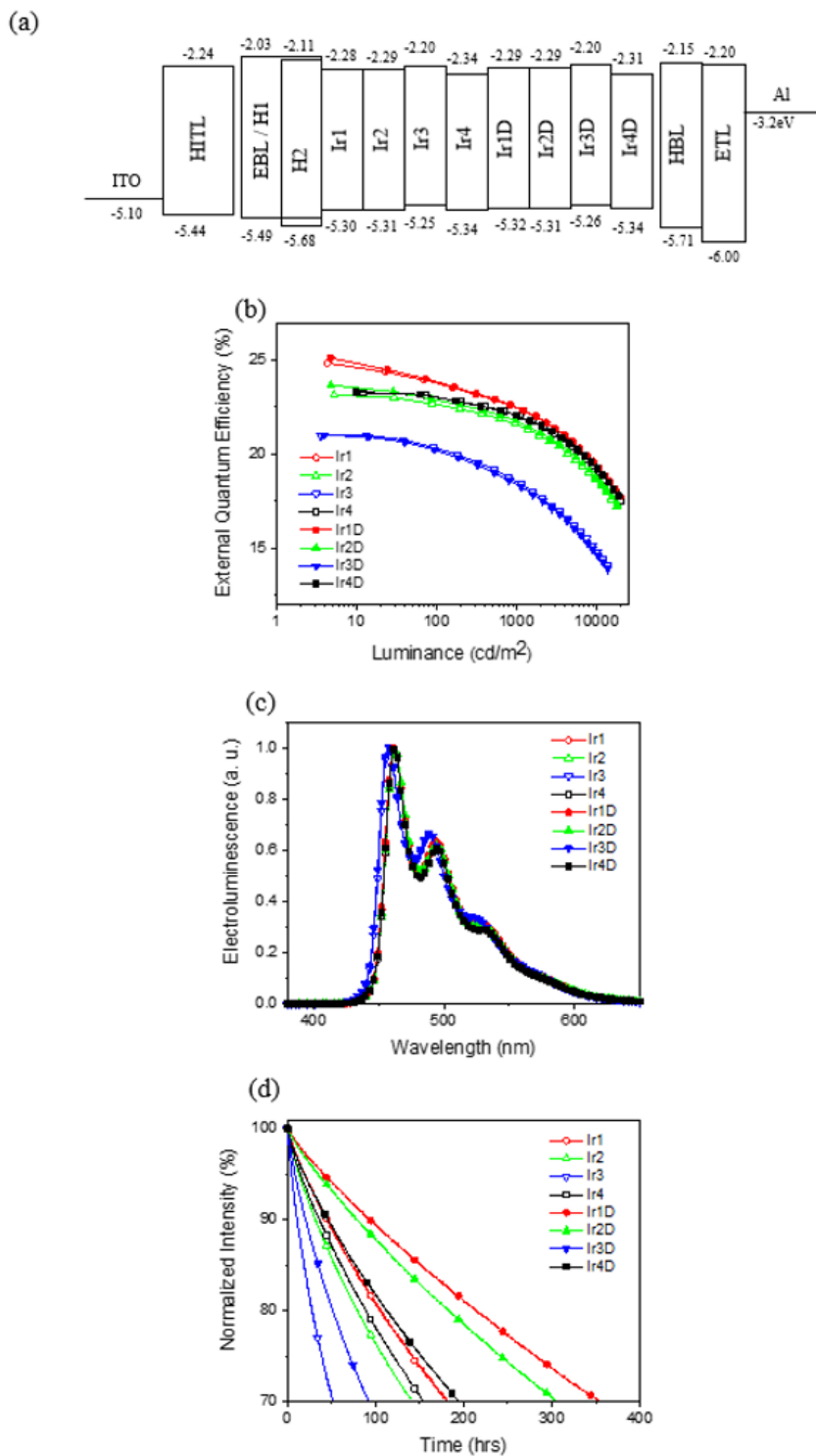


Figure 4

Device performances. (a) Energy level diagram of optimized device structures (unit of energy: eV), (b) external quantum efficiency as a function of luminance(cd/m^2), (c) normalized electroluminescence spectra and (d) normalized EL intensity vs. operational life time at $1000 \text{ cd}/\text{m}^2$ for each Ir complexes doped OLED devices.

Supplementary Files

This is a list of supplementary files associated with this preprint. Click to download.

- [SupplementaryInformation.docx](#)
- [SupplementaryInformation.docx](#)